Smart Materials and Structures

PAPER

Analytical coupled modeling of a magneto-based acoustic metamaterial harvester

To cite this article: H Nguyen *et al* 2018 *Smart Mater. Struct.* **27** 055010

IOP Publishing Smart Materials and Structures
Smart Mater. Struct. 27 (2018) 055010 (10pp) https://doi.org/10.1088/1361-665X/aab993

Analytical coupled modeling of a magneto-based acoustic metamaterial harvester

H Nguyen[1], R Zhu[1,2], J K Chen[1], S L Tracy[3] and G L Huang[1]

[1] Department of Mechanical & Aerospace Engineering, University of Missouri, Columbia, MO 65211, United States of America
[2] Department of Mechanics, Beijing Institute of Technology, Beijing 100081, People's Republic of China
[3] WorkSpace Futures, Steelcase Inc., Grand Rapids, MI 49508, United States of America

E-mail: huangg@missouri.edu

Received 8 December 2017, revised 14 February 2018
Accepted for publication 26 March 2018
Published 20 April 2018

Abstract

Membrane-type acoustic metamaterials (MAMs) have demonstrated unusual capacity in controlling low-frequency sound transmission, reflection, and absorption. In this paper, an analytical vibro-acoustic-electromagnetic coupling model is developed to study MAM harvester sound absorption, energy conversion, and energy harvesting behavior under a normal sound incidence. The MAM harvester is composed of a prestressed membrane with an attached rigid mass, a magnet coil, and a permanent magnet coin. To accurately capture finite-dimension rigid mass effects on the membrane deformation under the variable magnet force, a theoretical model based on the deviating acoustic surface Green's function approach is developed by considering the acoustic near field and distributed effective shear force along the interfacial boundary between the mass and the membrane. The accuracy and capability of the theoretical model is verified through comparison with the finite element method. In particular, sound absorption, acoustic-electric energy conversion, and harvesting coefficient are quantitatively investigated by varying the weight and size of the attached mass, prestress and thickness of the membrane. It is found that the highest achievable conversion and harvesting coefficients can reach up to 48%, and 36%, respectively. The developed model can serve as an efficient tool for designing MAM harvesters.

Keywords: acoustic metamaterial harvester, vibroacoustic coupling, membrane model, sound absorption, magnet damping

(Some figures may appear in colour only in the online journal)

1. Introduction

Low-frequency noise (audible sound waves) greatly threatens human health and is a major form of wasted energy. Compared to high-frequency noise, low-frequency noise spreads with modest attenuation through air, is often able to penetrate thick barriers with ease, and is not always easy to control. Based on the conventional mass density law, heavy and massive dissipative materials are needed to decrease low frequency sound transmission; however, lighter weight and compact size are always more desirable characteristics for real-world applications. New tools to control the propagation of these sound waves in the form of new materials are extremely desirable.

Recently, a membrane-type acoustic metamaterial (MAM) comprised of a thin subwavelength-scale microstructure was suggested for low-frequency sound attenuation [1–5]. This type of acoustic metamaterial has attracted large interest in the research community because it has a relatively simple geometry combined with an intriguing capability to dissipate low-frequency sound waves based on the local resonant mechanism. Based on the MAM design, the lightweight simple structures [6, 7] which expose broadband attenuation, and pure flexible design [8] have been proposed. Compared with conventional sound attenuation materials typically utilizing thermally-coupled dissipation mechanisms and suffering from inadequate low frequency sound attenuation, MAMs can be designed to possess nearly total reflection and/or absorption for targeting low-frequency acoustic sources.

The basic structure of this MAM consists of a prestressed membrane with one or multiple attached, small, heterogeneous

masses acting as resonators. The unusual low-frequency vibroacoustic behavior has been completely characterized, and the response spectrum shows separate transmission and absorption peaks around resonances [9, 10]. The low-frequency sound transmission mechanism has also been numerically explained through effective mass density and averaged normal displacement by using the finite element method, although the nearly total reflection and absorption of the MAM is of limited frequency bandwidth.

As one of many potential engineering applications, lightweight MAM honeycomb panels have been designed numerically and experimentally to mitigate low frequency noise specifically in aerospace structures [11]. For passive acoustic metamaterials, the operative wave frequencies are hardly adjustable once fabricated. Thus, they cannot adapt to real-life scenarios under ambient environments. One promising way to mitigate these problems is to incorporate an active element. Chen *et al* used a gradient magnetic field to actively tune the MAMs [12]. Xiao *et al* also investigated acoustic properties of membrane-type metamaterials actively adopted by external voltage to illustrate phase modulation and acoustic wave switch [13].

In another vein, scientists and engineers have been strongly interested in potential applications of acoustic metamaterials in the field of energy harvesting. The unique ability of acoustic metamaterials to trap acoustic waves in a localized regime can be used to efficiently harvest sound energy through integrating smart elements and electric circuits. From a practical point of view, there is combined value in both protecting people from damaging sound as well as actively retrieving energy from these noises to provide power to electronic devices without the need of batteries. As one of several candidate materials, piezoelectric materials have been successfully used in acoustic metamaterials for harvesting structure-borne as well as air-borne sound energies [14–19]. Although piezoelectric materials can generate a relatively high-voltage output from external motion-induced mechanical strain, the high impedance in piezoelectric-based harvesters mandates the load impedance to be high, which will significantly limit the acoustic energy harvesting efficiency [20–22]. Beside employing piezoelectric materials on designing harvesting structures, the voltage-tunable [23] and dielectric elastomer based [24] designs are also taken a lot of attention. Although these designs show very good ability on acoustic absorption, the harvested energy and ability on harvesting acoustic energy have not mentioned yet.

An alternative way to design an energy harvester is based on electromagnetic energy conversion, which is suitable for a low impedance and therefore can generate a high output current [25]. Mikoshiba *et al* [26] designed an acoustic metamaterial consisting of a spring-loaded magnet enclosed in a capped poly(methyl methacrylate) tube equipped with copper coils to harvest vibrational energy using electromagnetic induction. Ma *et al* [4] demonstrated a membrane acoustic metasurface that can convert the acoustic energy to electric current through electromagnetic induction with a power conversion efficiency of 23%, which demonstrates great potential for acoustic energy harvesting. However, many design issues have yet to be resolved and better understood such as enhancing efficiency, optimizing microstructures, and operating at a frequency bandwidth. A solid analytical model that can accurately capture the complicated vibro-acoustic-electromagnetic coupling behavior is greatly needed. The analytical method can provide both computational efficiency and flexibility, and therefore can be very useful in the design of multifunctional MAMs for desired engineering applications.

In this paper, we developed a comprehensive vibro-acoustic-electromagnetic coupling model to accurately capture the dynamic behavior as well as the energy absorption, conversion and harvesting in the proposed MAM harvester. Based on the model, sound absorption, acoustic-electronic energy conversion, and the MAM harvesting coefficient are quantitatively evaluated for various geometries and constitutive material properties of the metamaterial. The efficiencies of energy conversion and energy harvesting, the maxima of which are 48% and 36%, respectively, are analyzed and optimized by varying the subwavelength-scale microstructure and connected circuit configurations. Numerical simulations are conducted to validate the analytical solutions, and excellent agreement is observed.

2. Analytical modeling of the magneto-based acoustic metamaterial harvester

Without loss of generality, the magneto-based acoustic metamaterial harvester is considered as a MAM with a circular mass attached at the center of the membrane, a torus-shape magnet wire attached to the mass, and a permanent magnet placed close to the magnet wire, as shown in figure 1(a). When the incident pressure wave excites the membrane, the mass and attached wire vibrate in the magnetic field generated by the permanent magnet, which will induce a current in the moving wire. Thus, an external magnetic force acting on the mass and wire is initiated to prevent the vibration of the mass and magnet wire accordingly. By connecting a resistor, R_l, which may function as electric devices, into the circuit, the acoustic energy can be dissipated through R_l. This energy is called harvested energy, and the resistor R_l can be called the external load. In addition, the magnet coil also has an internal resistance and hence called internal load denoted by R_i. The electric energy dissipated through R_i always becomes heat, and therefore, can be called wasted energy. By defining the conversion energy as the total electric energy absorbed by both R_i and R_l, and harvested energy as the electric energy absorbed by only R_l, the harvested energy is a part of the conversion energy and will be zero when external load is not used ($R_l = 0$).

In our study, we focus on characterizing the MAM sound absorption in the tube subjected to a plane normal sound wave and investigate the energy harvesting ability of the magneto-based acoustic metamaterial harvester. Perfectly absorbing boundary conditions (BCs) are assumed in both ends of the tube so that there are no multiple reflected waves to the MAM. First, the external magnetic force is obtained analytically by considering the interaction between the magnetic field and the moving electric circuit. Then, the vibro-acoustic-magnetic coupling behavior of the MAM is analyzed through

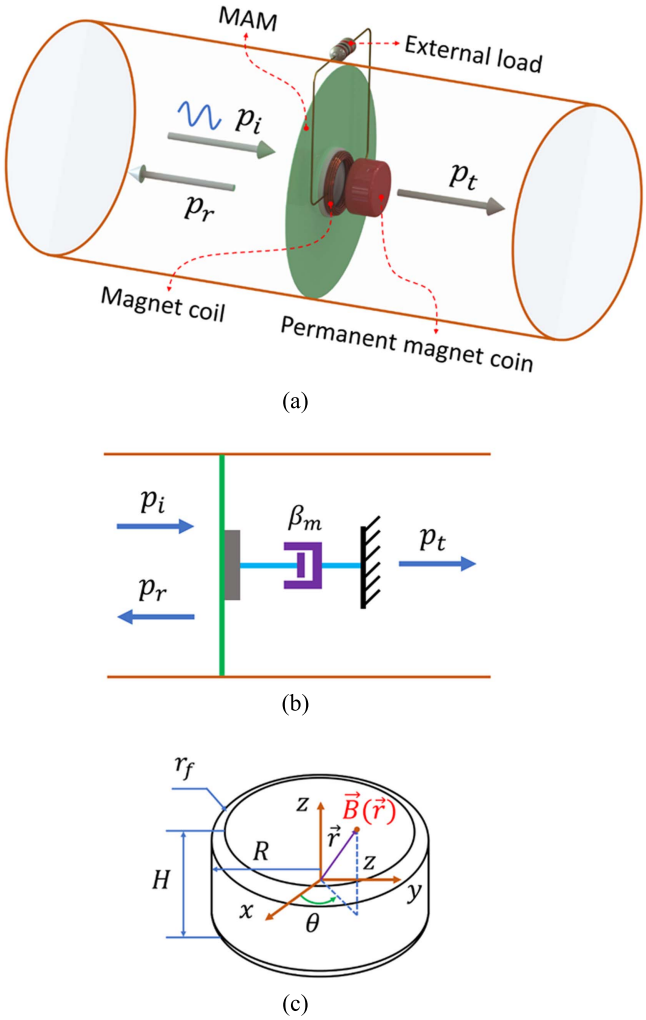

Figure 1. (a)—The model of the MAM harvester, (b)—the mechanical equivalent to the electromagnetic portion of the MAM harvester, (c)—the model of the permanent magnet coin.

the modal superposition theory, from which the sound transmission and reflection of the MAM can be analytically determined. Finally, the energy harvesting ability and its efficiency are quantitatively estimated by connecting electric circuits to the wire. This model can also be easily extended to analyze the MAM-based harvesters with multiple attached masses in arbitrary shapes.

2.1. The determination of magnetic force

For a permanent magnet coin, as shown in figure 1(c), the magnetic field around the magnet can be described as [27]

$$\vec{B}(\vec{r}) = \frac{\mu_0}{4\pi}\left\{\int_V \frac{(\nabla \times \vec{M}) \times (\vec{r} - \vec{r_V})}{|\vec{r} - \vec{r}_V|^3}\mathrm{d}V + \int_S \frac{(\vec{M} \times \vec{n}) \times (\vec{r} - \vec{r_S})}{|\vec{r} - \vec{r}_S|^3}\mathrm{d}S\right\}, \quad (1)$$

where, the magnetization $\vec{M}$ is constant in the $\vec{z}$ direction. Since the harvester is axisymmetric, only the magnetic field in the radial direction affects the motion of the harvester. Therefore, we rewrite B_r as

$$\begin{aligned} B_r(r,\ z) = {} & \frac{\mu_0}{4\pi}M \\ & \times \int_0^{2\pi}\int_{-\frac{H}{2}}^{-\left(\frac{H}{2}-r_f\right)} \frac{(z - z_s)\cos\varphi_s}{|r^2 + r_s^2 - 2rr_s\cos\varphi_s + (z - z_S)^2|^{3/2}} \\ & \times [R - r_f(1 - \cos\theta)]\mathrm{d}\varphi_s\mathrm{d}z_s \\ & + \frac{\mu_0}{4\pi}M\int_0^{2\pi}\int_{-\left(\frac{H}{2}-r_f\right)}^{\left(\frac{H}{2}-r_f\right)} \\ & \frac{(z - z_s)\cos\varphi_s}{|r^2 + r_s^2 - 2rr_s\cos\varphi_s + (z - z_S)^2|^{3/2}} \\ & \times R\mathrm{d}\varphi_s\mathrm{d}z_s + \frac{\mu_0}{4\pi}M \\ & \times \int_0^{2\pi}\int_{\left(\frac{H}{2}-r_f\right)}^{\frac{H}{2}} \frac{(z - z_s)\cos\varphi_s}{|r^2 + r_s^2 - 2rr_s\cos\varphi_s + (z - z_S)^2|^{3/2}} \\ & \times [R - r_f(1 - \cos\theta)]\mathrm{d}\varphi_s\mathrm{d}z_s, \end{aligned} \quad (2)$$

where, $\mu_0 = 4\pi \times 10^{-7}\,\mathrm{N\,A^{-2}}$ is the permeability of the free space; and $\sin\theta = \frac{\left[z_s \pm \left(\frac{H}{2} - r_f\right)\right]}{r_f}$, where '+' for the first integral and '−' for the third integral; R, H, r_f, and M are the radius, height, fillet radius, and magnetization of the permanent magnet, respectively.

When the mass and attached wire move back and forth inside the magnetic field $\vec{B}$ with velocity $\vec{v}$, the electromotive force induced inside the circuit reads

$$\epsilon = -\frac{\mathrm{d}\phi}{\mathrm{d}t} = \oint_L (\vec{v} \times \vec{B}) \cdot \mathrm{d}\vec{l} \approx N\oint_{\mathrm{loop}} (\vec{v} \times \vec{B}) \cdot \vec{s}\mathrm{d}l, \quad (3)$$

where $\vec{s}$ and N are the tangential vector and the number of the loops of the wire, respectively.

The current density induced inside the connected circuit is then

$$j = \frac{\epsilon}{A(R_i + R_l)}, \quad (4)$$

where the external resistor is denoted as R_l and the internal resistance of the magnet coil is $R_i = \frac{4N^2 d_o}{\sigma_c d_c^2}$ with the number of the loops of the wire being $N \approx \left(\frac{d_c}{d_w}\right)^2$ and d_o, d_w, d_c and σ_c are the diameters of the coil, magnet wire, the coil's cross-section and the electrical conductivity of the magnet wire, respectively.

Due to axisymmetric harvesting, the external distributed force acting on the wire can then be determined as

$$\vec{f_b} = \vec{j} \times \vec{B} = -\frac{\pi d_o N B_r^2 \dot{\mathscr{W}}_m}{A(R_i + R_l)}\vec{n}_z \quad (5)$$

herein, the radial component of the magnetic field is ignored since it will be canceled out in summation; d_c, A, $\vec{v}$ and $\dot{\mathscr{W}}_m$ are the diameter of the wire, cross-sectional area of the wire, the velocity vector of the mass and its z-directional component ($\dot{\mathscr{W}}_m = v_z$), respectively. Thus, the total induced magnetic force can be determined by summing the distributed

forces along the wire as

$$\vec{F}_m = \int_{\text{coil}} \vec{f}_b \,\mathrm{d}l = -\frac{(\pi d_o N B_r)^2}{R_i + R_l} \dot{\mathscr{W}}_m \vec{n}_z. \tag{6}$$

Since the magnetic force is proportional to the velocity of the mass, physically the magnetic force acts exactly like a damping force to the membrane with the magnet damping coefficient [28] being $\beta_m = \frac{(\pi d_o N B_r)^2}{R_i + R_l}$, as shown in the figure 1(b). In the frequency domain, the average power absorbed by the magnetic damper, therefore, can be calculated as

$$\begin{aligned} W_d &= \frac{\omega}{2\pi}\int_0^{2\pi/\omega} \mathcal{R}_e\{F_m\} \cdot \mathcal{R}_e\{\dot{\mathscr{W}}_m\}\,\mathrm{d}t \\ &= \frac{1}{2}\frac{(\pi d_o N B_r)^2}{R_i + R_l}\,|\dot{\mathscr{W}}_m|^2 = \frac{1}{2}\beta_m\,|\dot{\mathscr{W}}_m|^2. \end{aligned} \tag{7}$$

Note that, for the system without other energy dissipation, the electromagnetic part of the harvester should be equivalent to a mechanical damper that is proportional to the damping coefficient β_m.

By further analyzing the damping coefficient in the form of $\beta_m = \frac{(\pi d_o B_r)^2}{4d_o\,/\,(\sigma_c d_c^2) + R_l\,/\,N^2}$, we can conclude that the conversion coefficient depends on the ring diameter and ring cross-sectional diameter, and reaches its maximum value when zero load is applied.

$$\frac{\partial \mathscr{W}}{\partial r} = 0, \quad 2\pi\overline{V}(b) = m\ddot{\mathscr{W}}(b) \quad \text{at} \quad r = b, \tag{10}$$

where $\overline{D} = \frac{h^3}{12}\left(\sigma_0 + \frac{E}{1-\nu^2}\right)$ is the effective bending stiffness of the membrane, $T = \sigma h$ is the pretension in the membrane, and $\overline{V}(b)$ is the shear force at radius b [29]

$$\overline{V}(b) = V(b) + T\frac{\partial \mathscr{W}}{\partial r}\bigg|_{r=b}, \tag{11}$$

where $V(b)$, h and ρ are the Kirchhoff's shear force at the inner boundary, the thickness, and mass density of the annulus membrane, respectively.

The general solution of the equation (8) can be expressed as [29, 30]

$$\mathscr{W}(r) = AJ_0(\gamma_1 r) + BY_0(\gamma_1 r) + CI_0(\gamma_2 r) + DK_0(\gamma_2 r), \tag{12}$$

where

$$\gamma_{1,2} = \sqrt{\sqrt{\alpha^4 + \beta^4} \mp \alpha^2} \quad \alpha^2 = \frac{T}{2D} \quad \beta^4 = \frac{\rho h \omega^2}{\overline{D}}. \tag{13}$$

J_0, Y_0 and I_0, K_0 are the zero-order Bessel functions and modified Bessel functions, respectively.

Since only the steady-state response field will be considered, the time factor $\mathrm{e}^{\mathrm{i}\omega t}$, which applies to all the field variables, will be suppressed.

By using the BCs, the natural frequencies and mode shape functions of the MAM can be determined by solving the eigen-value problem of the matrix

$$\begin{vmatrix} J_0(\gamma_1 a) & Y_0(\gamma_1 a) & I_0(\gamma_2 a) & K_0(\gamma_2 a) \\ \gamma_1 J_1(\gamma_1 a) & \gamma_1 Y_1(\gamma_1 a) & -\gamma_2 I_1(\gamma_2 a) & \gamma_2 K_1(\gamma_2 a) \\ \gamma_1 J_1(\gamma_1 b) & \gamma_1 Y_1(\gamma_1 b) & -\gamma_2 I_1(\gamma_2 b) & \gamma_2 K_1(\gamma_2 b) \\ \gamma_1^3 J_1(\gamma_1 b) - \alpha J_0(\gamma_1 b) & \gamma_1^3 Y_1(\gamma_1 b) - \alpha Y_0(\gamma_1 b) & \gamma_1^3 I_1(\gamma_2 b) - \alpha I_0(\gamma_2 b) & -\gamma_2^3 K_1(\gamma_2 b) - \alpha K_0(\gamma_2 b) \end{vmatrix} = 0. \tag{14}$$

2.2. Coupling vibro-acoustic-electromagnetic model of the MAM

Since the attached mass and wire in the MAM are assumed to be perfectly bonded to the membrane and rigid compared with the deformable membrane, to properly capture effects of the finite mass on the small deformation of the membrane, the proposed MAM is decomposed into two parts: an annulus membrane and a mass with the attached magnet coil. Considering the elastic membrane here as an elastic plate, the governing equation of the annulus pre-tension membrane can be written as [10, 29]

$$\overline{D}\nabla^4 \mathscr{W} - T\nabla^2 \mathscr{W} - \rho h \omega^2 \mathscr{W} = 0 \tag{8}$$

with the BCs

$$\mathscr{W} = \frac{\partial \mathscr{W}}{\partial r} = 0, \quad \text{at} \quad r = a \tag{9}$$

Next, consider a plane sound wave is normally incident on the MAM. Per the fact that the thickness of the MAM is extremely small compared with the wavelength of low-frequency sound in air, thickness effects of the MAM can be ignored. The objective is to determine the acoustic energy reflection, transmission, and absorption within the MAM. The governing equation of the acoustic excited membrane based on the plate theory and motion equations of the mass can be expressed as

$$\overline{D}(1 + \mathrm{i}\omega\eta)\nabla^4 \mathscr{W} - T\nabla^2 \mathscr{W} - \rho\omega^2 \mathscr{W} = \Delta p + \overline{V}\delta(r - b) \tag{15}$$

$$-2\pi b\overline{V} + F_m + \int_{S_i} \Delta p \,\mathrm{d}S = -m\omega^2 \mathscr{W}(b), \tag{16}$$

where S_i denotes the circular surface of the mass, and Δp is the total pressure acting on the membrane

$$\Delta p = (p_i + p_r - p_t)|_{z=0} = 2\left[P_i - \mathrm{i}\omega\langle\mathscr{W}\rangle + \omega k_a Z_0 \times \int_S \delta G(r|r')\mathscr{W}(r')\mathrm{d}r'\right], \tag{17}$$

where S is the surface of the MAM; $Z_0 = \rho_0 c_0$ is the specific characteristic impedance of air; P_i is the amplitude of the incident pressure wave; $\langle\mathscr{W}\rangle$ is the average displacement of the membrane; and $\delta G(r|\ r')$ is the deviation of the acoustic Green's function of the tube measured at $z = 0$ [31]

$$\delta G(r|r') = \frac{1}{\pi a^2}\sum_{l=1}^{\infty}\frac{J_0(k_{rl}r)J_0(k_{rl}r')}{J_0^2(k_{rl}a)\sqrt{k_{rl}^2 - k_a^2}}, \tag{18}$$

where k_a is the wavenumber of air and k_{rl} is the lth order wavenumber of air in the radial direction of the waveguide.

The dissipative property of the membrane is employed here through the imaginary part of the Young's modulus, viscosity χ, and effective loss factor η of the membrane as

$$E_m = E + \mathrm{i}\omega\chi \quad \eta = \frac{\chi}{E + (1 - \nu^2)\sigma_0}, \tag{19}$$

where E and σ_0 are the Young's modulus and prestress of the membrane.

The superposition method is adopted by assuming the solution in the form

$$\mathscr{W}(r) = \sum_k \lambda_k \mathscr{W}_k(r), \tag{20}$$

where $\mathscr{W}_k(r)$ is the kth eigen function of the annulus membrane.

Multiplying $\mathscr{W}_n$ in equation (15) and conducting an integral over the surface of the annulus membrane S_o lead to

$$\begin{aligned}&\textstyle\sum_k \lambda_k\Bigg\{\mathrm{i}\omega\eta T\int_{S_o}\mathscr{W}_n\nabla^2\mathscr{W}_k\mathrm{d}S_o + \delta_{n,k}(\omega_k^2 + \mathrm{i}\omega_k^2\eta\omega - \omega^2)\\ &\times\left[\rho h\int_{S_o}\mathscr{W}_n^2\mathrm{d}S_o + m\mathscr{W}_n^2(b)\right] + \mathrm{i}\omega\beta_m\mathscr{W}_n(b)\mathscr{W}_k(b)\\ &+ 2\mathrm{i}\pi a^2\omega Z_0\langle\mathscr{W}_n\rangle\langle\mathscr{W}_k\rangle - \frac{2\mathrm{i}\omega k_a Z_0}{\pi a^2}\\ &\times\sum_{l=1}^{\infty}\frac{\int_S J_0(k_{rl}r)\mathscr{W}_n(r)\mathrm{d}r\int_S J_0(k_{rl}r')\mathscr{W}_k(r')\mathrm{d}r'}{J_0^2(k_{rl}a)\sqrt{k_{rl}^2 - k_a^2}}\Bigg\}\\ &= 2\pi a^2 P_i\langle\mathscr{W}_n\rangle.\end{aligned} \tag{21}$$

The equation (21) is recognizable as a system of linear equations where unknown variables λ_k can be numerically determined.

Therefore, the far field transmission, reflection coefficients and absorption for radiated plane waves of the MAM can be expressed as

$$T = \frac{\mathrm{i}\omega Z_0}{P_i}\sum_k \lambda_k\langle\mathscr{W}_k\rangle \quad R = 1 - T \quad A = 1 - |R|^2 - |T|^2, \tag{22}$$

respectively.

For the acoustic energy characterization, the acoustic input energy is calculated as

$$W_{\mathrm{in}} = \frac{\pi a^2\ |P_i|^2}{2Z_0} \tag{23}$$

and the energy absorbed by the elastic membrane, or elastic absorption (due to deformable elastic dissipation), which can be determined by subtracting the energy absorbed by the magnetic damper and the elastic absorption coefficient, are presented as

$$W_m = A \cdot W_{\mathrm{in}} - W_d \quad A_m = \frac{W_m}{W_{\mathrm{in}}} = A - \frac{W_d}{W_{\mathrm{in}}}, \tag{24}$$

respectively. On the other side, the harvested energy through connecting the external resistor R_l is

$$W_h = \frac{R_l}{R_i + R_l}W_d. \tag{25}$$

The acoustic energy conversion coefficient which corresponds to the total electric energy (W_d), and harvesting coefficient which only corresponds to the amount of electric energy harvested through the external load R_l (W_h) can be defined as

$$c = \frac{W_d}{W_{\mathrm{in}}} \quad \varphi = \frac{W_h}{W_{\mathrm{in}}} = \frac{R_l}{R_i + R_l}c. \tag{26}$$

3. Results and discussion

To verify the theoretical model of the MAM harvester, several configurations of theoretically-derived acoustic absorption analyses are compared with simulation results derived from the commercial code, COMSOL Multiphysics. Since the magnetic field generated from the permanent magnet is stationary, a two-step study is employed in the numerical simulation. In the first step, a 'Stationary' study on the 'Magnetic Fields, No Currents' module is selected to obtain the static permanent magnetic field. In the second step, a 'Frequency Domain' on the 'Acoustic-Structure Interaction' module is performed to study the interaction between acoustic domains and MAM. The magnetic effect is considered by applying a velocity-dependent body force on the magnet coil calculated from the magnetic field and the mass' velocity. The MAM parameters used in analytical modeling and numerical simulation are listed in the table 1. The diameter of the magnet wire is set to 0.104 mm, and the internal resistance of the magnet coil R_i, therefore, is equal to 0.55 Ω.

To validate the theoretical model, the two major results predicted by the theoretical analysis and numerical simulation are compared. First, we compare the magnetic fields measured at the center of the magnet coil's cross-section B_r by employing equation (2) versus COMSOL methods. The results for B_r are −0.29278 T and −0.29267 T respectively, which shows the tremendous accuracy of the theoretical magnet calculation. Second, we compare the wave absorption of the MAM harvester predicted from the theoretical analysis versus the numerical simulation based on the commercial

Table 1. The MAM harvester's parameters.

Element	Property	Symbol	Value
Elastic membrane	Radius	a	25 mm
	Thickness	h	0.1 mm
	Young's modulus	E	1.9×10^6 Pa
	Poisson's ratio	ν	0.48
	Mass density	ρ	980 kg m^{-3}
	Prestress	σ_0	2.2×10^5 Pa
	Viscosity	χ	796 Pa s
Attached mass	Radius	b	5 mm
	Thickness	t	0.35 mm
	Mass density	ρ_m	2900 kg m^{-3}
Permanent magnet coin	Radius	R	3 mm
	Height	H	3 mm
	Fillet radius	r_f	0.375 mm
	Magnetization	M	750 kA m^{-1}
Magnet coil	Diameter of the coil	d_o	6 mm
	Diameter of the magnet coil's cross-section	d_c	0.4 mm
	The gap in between the mass and the permanent magnet	Δ	0.5 mm
	Electrical conductivity	σ_c	6×10^7 S m^{-1}
	Mass density	ρ_w	8960 kg m^{-3}

code COMSOL Multiphysics as shown in the figure 2. Three cases of the harvester are: (1) viscous membrane (elastic membrane with dissipative property) but without magnet effect; (2) non-viscous membrane with magnet effect; and (3) both viscous membrane and the magnet effect. The results from the theoretical analysis and the simulation are nearly perfectly matched. The developed theoretical analysis therefore is highly precise and correlates extremely well with numerical simulation. Furthermore, while the dissipated energy from the viscous membrane is very small (less than 5%), the absorption of the harvester under the magnet effect is significantly improved (34%). The proposed harvester configuration thus demonstrates a very high potential to harvest energy. Next, the theoretical analysis is employed to analyze the parameter effect and further optimize the harvester.

Figures 3(a) and (b) show the effect of the external load R_l on the conversion and harvesting coefficients of the MAM harvester. In the figures, the material parameters of the MAM are the same as those listed in table 1. Through analysis we have shown that the conversion coefficient, which corresponds to the amount of energy absorbed by the circuit, decreases when the external load R_l increases. The best conversion coefficient is observed when the external load is zero. This phenomenon is explained by considering the effect of the magnet damping coefficient β_m: an increased external load R_l will lower the magnet damping coefficient, which reduces the dissipated energy through the circuit.

This figure also shows that all the conversion coefficient peaks are located in the hybridized resonant frequency [4], 198 Hz. Due to small elastic dissipative energy (elastic absorption), the conversion coefficient and the absorption peaks of the harvester are at very close frequencies. The conversion peak here matches with the first absorption peak at the hybridized resonant frequency, which is very close to the first anti-resonant frequency. The first anti-resonance, on the other hand, occurs when the real part of the acoustic Green's function of the MAM [4] is equal to zero and completely depends on the first two resonant frequencies. The dissipative property of the membrane and the magnet damping coefficient are only related to the resistance of the harvester and will not contribute to the resonant frequencies, which is also confirmed from the absence of these factors in the characteristic equation (14). Therefore, the peak conversion coefficient in the hybridized resonant frequency will not change when the external loads are varied. The harvesting coefficient φ of the harvester presented in figure 3(b), which is defined as the amount of the energy harvested through the external load R_l, on the other hand, does not follow the trend of the conversion coefficient. It will initially increase, then reach the best performance when $R_l/R_i \approx 1.25$, and afterward decrease with the increase the external load. The harvested energy depends not only on the ratio of external load to internal load (R_l/R_i) as shown in the equation (25), but also on the amount of acoustic energy converted to electric energy. The increase of R_l will lower the magnet damping coefficient β_m, and therefore make the conversion energy decrease. Therefore, the increase of the external load R_l does not ensure the harvested energy is increased as observed in figure 3(b). In addition, since the harvested energy is proportional to the conversion energy (see the equation (26)), the peak of the harvesting coefficient is also located at the hybridized resonant frequency.

The next geometric parameter studied is the thickness of the membrane h. The thing learnt from the previous discussion is the lower external load R_l, which leads to higher magnet damping coefficient β_m, the higher conversion coefficient c. Therefore, to get the highest conversion coefficient, the external load R_l is set to be zero. The other parameters are kept the same as listed in table 1. When the membrane becomes thicker (or h increases), the effective bending stiffness of the membrane $\overline{D}$ increases, which theoretically makes the resonant frequencies of the harvester also increase. Consequently, the peaks of the conversion coefficient and the elastic dissipative energy through the membrane shift to higher frequencies as observed in figures 4(a) and (b). When the membrane becomes thicker, the amplitude of the conversion coefficient peak gradually decreases. The amplitude of the elastic dissipative coefficient peak, in the other hand, gradually increases with the increase of the thickness of membrane since the conversion energy partially converts to elastic energy due to the increase of the strain energy [10]. As we can expect physically, the effective bending stiffness of the membrane will be significantly enhanced with the increase of the thickness of the membrane, as a consequence, the stored strain energy and the elastic dissipative energy in the

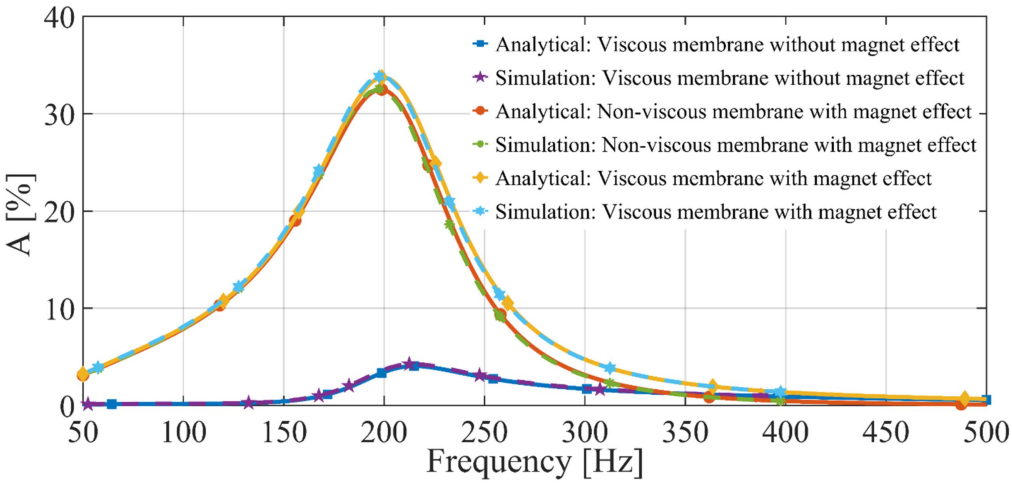

Figure 2. Comparisons between the simulation and analytical results for the cases: the membrane with dissipative property but without effect of the magnet, the membrane without dissipative property but with the magnet effect, the membrane with both dissipative property and the magnet effect.

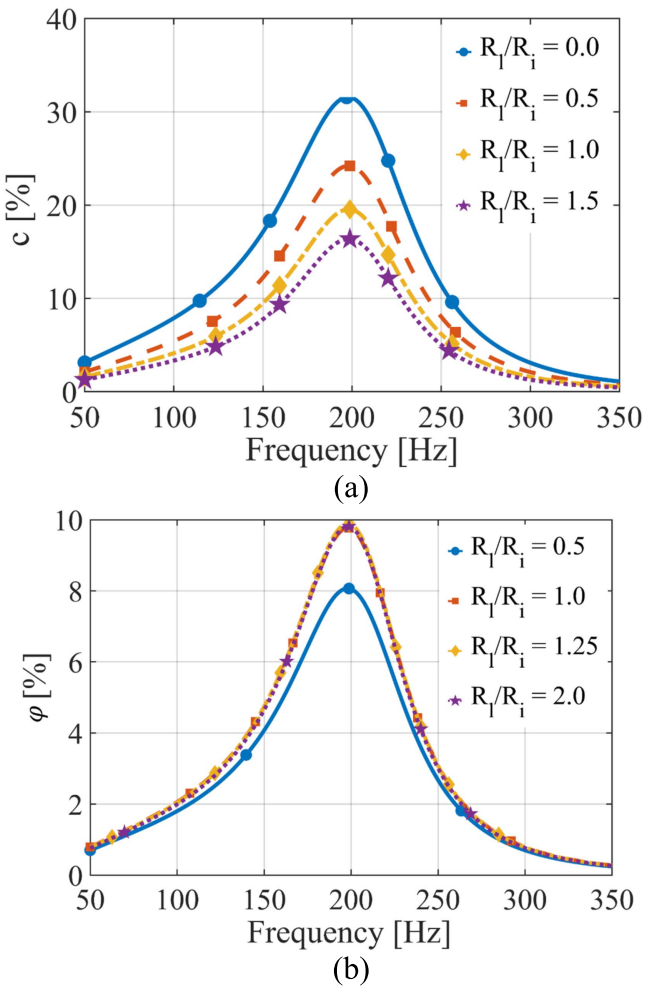

Figure 3. The effect of the external load on the conversion (a) and harvesting (b) coefficients.

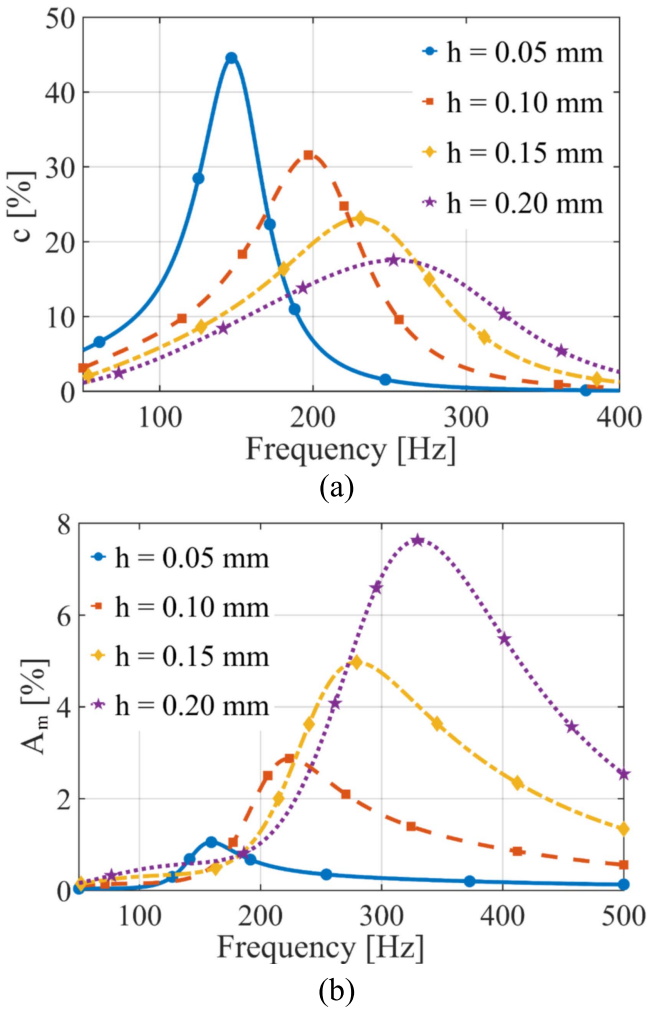

Figure 4. The effect of the membrane's thickness on the conversion coefficient of the harvester (a) and the elastic dissipative energy of the membrane (b).

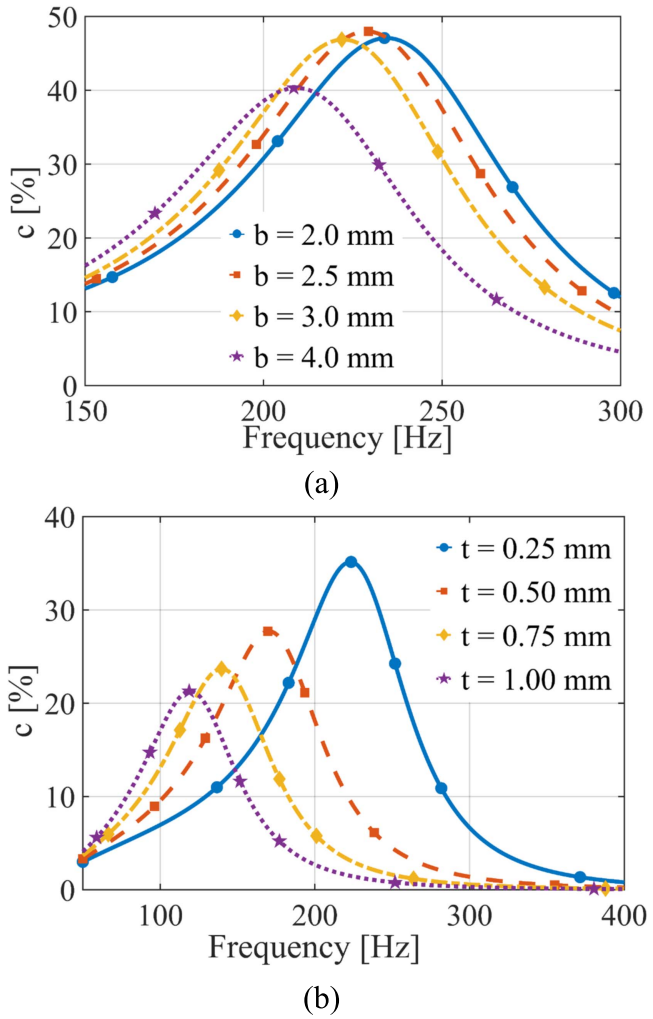

Figure 5. The effect of the mass' dimensions on the conversion coefficient of the harvester.

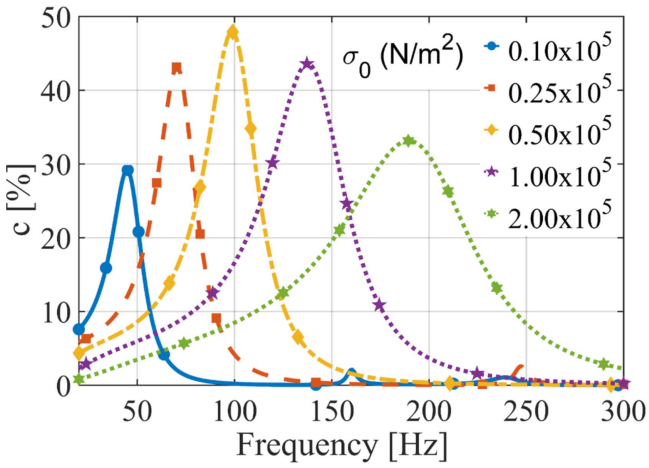

Figure 6. The effect of the membrane's prestress on the conversion coefficient.

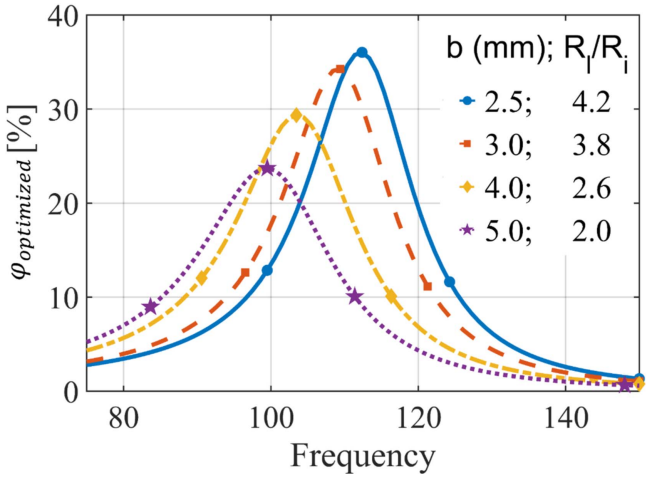

Figure 7. The optimized harvesting coefficient of the harvester for $\sigma_0 = 0.5 \times 10^5\,\mathrm{N\,m^{-2}}$.

membrane will be enlarged, as illustrated in figure 4(b). On the other hand, a harder membrane sometimes prevents the motion of the mass, which can result in a lower magnetic effect and lowers conversion coefficient as presented in figure 4(a).

The contribution of the mass' dimensions on the conversion coefficient is presented in the figures 5(a) and (b). In the study, the external load R_l is set to be zero and the other parameters are the same as listed in table 1. It is observed that with the increase of the mass radius b or thickness t, the resonant frequencies of the harvester will decrease due to increase of the mass weight leading to a corresponding shift in the conversion coefficient peak's position. While the conversion coefficient peak is clearly lowered when the mass' thickness t is increased, it will initially increase when the mass' radius b increases, then reach the best value at $b = 2.5$ mm, and continually decrease afterwards. Note that, to the best of our knowledge, the best conversion coefficient peak of 48% observed at $b = 2.5$ mm is much larger than conversion coefficients possible in a thin MAM. Furthermore, the corresponding absorption peak is nearly 50%, equal to the limit of the absorption capacity for a thin MAM harvester [10].

In addition to geometric parameters, we investigated the influence of the membrane's prestress on the conversion coefficient under free external load as shown in figure 6. In this study, all parameters other than the prestress σ_0 are the same as listed in table 1. While the prestress is varied from 0.1×10^5 to $2.0 \times 10^5\,\mathrm{N\,m^{-2}}$, the membrane's effective bending stiffness $\overline{D}$ increases, and the resonant frequencies of the harvester thus also increase. The conversion coefficient peak also shifts to the higher frequency correspondingly. In contrast to the effects of the membrane's thickness h on the effective bending stiffness $\overline{D}$ (proportional to h^3), the prestress, which is only linear function of the bending stiffness, can only have a moderate effect on the elastic membrane's strain energy and hence the elastic dissipative energy [10]. Therefore, the amplitude of the conversion coefficient peak, instead of decreasing continuously like observed from figure 4(a) while the prestress increases, gradually reaches a best value of 48% when $\sigma_0 = 0.5 \times 10^5\,\mathrm{N\,m^{-2}}$, and then deceases gradually. It can be understood that the membrane

with an optimized value of prestress leads to a very high magnet effect, and hence results in the best conversion coefficient. This state of membrane, therefore, is generally called 'acoustic impedance matching' [18].

Based on these parameter analyses, we optimized the energy harvester design. Due to the complex of the multiple value optimization, in this study, only two parameters: the external load R_l and the radius of the mass b are selected. In this study the prestress $\sigma_0 = 0.5 \times 10^5\,\mathrm{N\,m^{-2}}$ is selected. While other parameters are kept the same as listed in the table 1, two parameters (the mass' radius and the external load R_l) are varied to find the optimized harvesting coefficient. Figure 7 shows the optimized harvesting coefficients corresponding to several values of the given mass radius b and optimized value of the external load R_l. We observed that the maximum harvesting coefficient peak is 36% while the possible capacity of the harvester is no more than 50%. It can be realized that with a given value of b, there will have a corresponding optimized value of R_l or R_l/R_i. The result indicates that increasing b will lower the optimized value of R_l/R_i. Lowering the ratio R_l/R_i makes the portion of the harvested energy in the total electric energy or conversion energy decreased. As a result, the harvesting coefficient can be decreased as shown in the figure 7.

In this paper, the MAM harvester is based on axisymmetric model, which can produce elegant analytical solutions for both homogeneous and inhomogeneous problems. Based on the model, the parameter effect and optimization can easily be conducted. The similar approach can easily be extended for other types of structures such as rectangular MAMs or MAMs with multiple attached masses. However, for the cases with the general geometries, the point-matching method should be employed to numerically solve the governing equations and determine the magnet force [9, 10].

4. Conclusion

In this work, an analytical model of a magneto-based MAM harvester is proposed, which shows substantial improvement in all absorption, conversion, and harvesting coefficients. By investigating the contribution of the geometric parameters and membrane's prestress on the acoustic performance of the harvester, it is shown that the absorption can reach the absorption limit of a thin MAM (50%), the conversion coefficient can reach to 48%; and the harvested coefficient can also reach to a very impressive number, 36%. Furthermore, the theoretical analysis has been well validated by comparing to numerical simulation results generated using the commercial code COMSOL Multiphysics. These results lay a strong foundation for developing acoustic metamaterial harvesters and show tremendous application potential for the proposed MAM harvester.

Acknowledgments

This work was partially supported by Steelcase Inc.

ORCID iDs

G L Huang https://orcid.org/0000-0003-0959-8427

References

[1] Yang Z, Mei J, Yang M, Chan N H and Sheng P 2008 Membrane-type acoustic metamaterial with negative dynamic mass *Phys. Rev. Lett.* **101** 204301
[2] Yang Z, Dai H M, Chan N H, Ma G C and Sheng P 2010 Acoustic metamaterial panels for sound attenuation in the 50–1000 Hz regime *Appl. Phys. Lett.* **96** 041906
[3] Mei J, Ma G, Yang M, Yang Z, Wen W and Sheng P 2012 Dark acoustic metamaterials as super absorbers for low-frequency sound *Nat. Commun.* **3** 756
[4] Ma G, Yang M, Xiao S, Yang Z and Sheng P 2014 Acoustic metasurface with hybrid resonances *Nat. Mater.* **13** 873–8
[5] Huang T Y, Shen C and Jing Y 2016 Membrane- and plate-type acoustic metamaterials *J. Acoust. Soc. Am.* **139** 3239–49
[6] Ma F Y, Huang M and Wu J H 2017 Acoustic metamaterials with synergetic coupling *J. Appl. Phys.* **122** 215102
[7] Ma F, Huang M and Wu J H 2017 Ultrathin lightweight plate-type acoustic metamaterials with positive lumped coupling resonant *J. Appl. Phys.* **121** 015102
[8] Ma F, Wu J H, Huang M, Zhang W and Zhang S 2015 A purely flexible lightweight membrane-type acoustic metamaterial *J. Phys. D: Appl. Phys.* **48** 175105
[9] Chen Y Y, Huang G L, Zhou X M, Hu G K and Sun C T 2014 Analytical coupled vibroacoustic modeling of membrane-type acoustic metamaterials: membrane model *J. Acoust. Soc. Am.* **136** 969–79
[10] Chen Y Y, Huang G L, Zhou X M, Hu G K and Sun C T 2014 Analytical coupled vibroacoustic modeling of membrane-type acoustic metamaterials: plate model *J. Acoust. Soc. Am.* **136** 2926–34
[11] Sui N, Yan X, Huang T-Y, Xu J, Yuan F-G and Jing Y 2015 A lightweight yet sound-proof honeycomb acoustic metamaterial *Appl. Phys. Lett.* **106** 171905
[12] Chen X, Xu X, Ai S, Chen H, Pei Y and Zhou X 2014 Active acoustic metamaterials with tunable effective mass density by gradient magnetic fields *Appl. Phys. Lett.* **105** 071913
[13] Xiao S, Ma G, Li Y, Yang Z and Sheng P 2015 Active control of membrane-type acoustic metamaterial by electric field *Appl. Phys. Lett.* **106** 091904
[14] Airoldi L and Ruzzene M 2011 Design of tunable acoustic metamaterials through periodic arrays of resonant shunted piezos *New J. Phys.* **13** 113010
[15] Chen S-B, Wen J-H, Yu D-L, Wang G and Wen X-S 2011 Band gap control of phononic beam with negative capacitance piezoelectric shunt *Chin. Phys.* B **20** 014301
[16] Gonella S, To A C and Liu W K 2009 Interplay between phononic bandgaps and piezoelectric microstructures for energy harvesting *J. Mech. Phys. Solids* **57** 621–33
[17] Bergamini A, Delpero T, De Simoni L, Di Lillo L, Ruzzene M and Ermanni P 2014 Phononic crystal with adaptive connectivity *Adv. Mater.* **26** 1343–7
[18] Li J, Zhou X, Huang G and Hu G 2016 Acoustic metamaterials capable of both sound insulation and energy harvesting *Smart Mater. Struct.* **25** 045013
[19] Akl W and Baz A 2013 Active acoustic metamaterial with simultaneously programmable density and bulk modulus *J. Vib. Acoust.* **135** 031001
[20] Roundy S and Wright P K 2004 A piezoelectric vibration based generator for wireless electronics *Smart Mater. Struct.* **13** 1131–42

[21] Aridogan U, Basdogan I and Erturk A 2016 Random vibration energy harvesting on thin plates using multiple piezopatches *J. Intell. Mater. Syst. Struct.* **27** 2744–56
[22] Tol S, Degertekin F L and Erturk A 2017 Structurally embedded reflectors and mirrors for elastic wave focusing and energy harvesting *J. Appl. Phys.* **122** 164503
[23] Xiao S, Tang S T and Yang Z 2017 Voltage-tunable acoustic metasheet with highly asymmetric surfaces *Appl. Phys. Lett.* **111** 194101
[24] Lu Z B, Shrestha M and Lau G K 2017 Electrically tunable and broader-band sound absorption by using micro-perforated dielectric elastomer actuator *Appl. Phys. Lett.* **110** 182901
[25] Zhang Q and Kim E S 2014 Vibration energy harvesting based on magnet and coil arrays for watt-level handheld power source *Proc. IEEE* **102** 1747–61
[26] Mikoshiba K, Manimala J M and Sun C T 2013 Energy harvesting using an array of multifunctional resonators *J. Intell. Mater. Syst. Struct.* **24** 168–79
[27] Griffiths D J 2013 *Introduction to Electrodynamics* (Boston: Pearson)
[28] Nagaya K, Kojima H, Karube Y and Kibayashi H 1984 Braking forces and damping coefficients of eddy current brakes consisting of cylindrical magnets and plate conductors of arbitrary shape *IEEE Trans. Magn.* **20** 19
[29] Leissa A W 1969 *Vibration of Plates* (Washington: Scientific and Technical Information Division, NASA)
[30] Graff K F 1991 *Wave Motion in Elastic Solids* (New York: Dover)
[31] Ingard U 1954 Transmission of sound through a stretched membrane *J. Acoust. Soc. Am.* **26** 99–101